Cell Reports
Article

Antibody 8ANC195 Reveals a Site of Broad Vulnerability on the HIV-1 Envelope Spike

Louise Scharf,[1] Johannes F. Scheid,[2,7] Jeong Hyun Lee,[3,7] Anthony P. West, Jr.,[1] Courtney Chen,[1] Han Gao,[1] Priyanthi N.P. Gnanapragasam,[1] René Mares,[1] Michael S. Seaman,[4] Andrew B. Ward,[3] Michel C. Nussenzweig,[2,5] and Pamela J. Bjorkman[1,6,*]

[1]Division of Biology and Biological Engineering, California Institute of Technology, Pasadena, CA 91125, USA
[2]Laboratory of Molecular Immunology, The Rockefeller University, New York, NY 10065, USA
[3]Department of Integrative Structural and Computational Biology, The Scripps Research Institute, La Jolla, CA 92037, USA
[4]Beth Israel Deaconess Medical Center, Boston, MA 02215, USA
[5]Howard Hughes Medical Institute, The Rockefeller University, New York, NY 10065, USA
[6]Howard Hughes Medical Institute, California Institute of Technology, Pasadena, CA 91125, USA
[7]These authors contributed equally to this work
*Correspondence: bjorkman@caltech.edu
http://dx.doi.org/10.1016/j.celrep.2014.04.001

SUMMARY

Broadly neutralizing antibodies (bNAbs) to HIV-1 envelope glycoprotein (Env) can prevent infection in animal models. Characterized bNAb targets, although key to vaccine and therapeutic strategies, are currently limited. We defined a new site of vulnerability by solving structures of bNAb 8ANC195 complexed with monomeric gp120 by X-ray crystallography and trimeric Env by electron microscopy. The site includes portions of gp41 and *N*-linked glycans adjacent to the CD4-binding site on gp120, making 8ANC195 the first donor-derived anti-HIV-1 bNAb with an epitope spanning both Env subunits. Rather than penetrating the glycan shield by using a single variable-region CDR loop, 8ANC195 inserted its entire heavy-chain variable domain into a gap to form a large interface with gp120 glycans and regions of the gp120 inner domain not contacted by other bNAbs. By isolating additional 8ANC195 clonal variants, we identified a more potent variant, which may be valuable for therapeutic approaches using bNAb combinations with nonoverlapping epitopes.

INTRODUCTION

The only target of neutralizing anti-HIV-1 antibodies is the envelope glycoprotein (Env) spike, a heterotrimer of gp120 and gp41 subunits. Single-cell-based antibody cloning techniques have recently uncovered a large number of antibodies that can potently neutralize highly diverse HIV-1 variants by targeting Env (Burton et al., 2012; Klein et al., 2013b; Mascola and Haynes, 2013; Scheid et al., 2011; Wu et al., 2010). When transferred passively, broadly neutralizing antibodies (bNAbs) can prevent infection by HIV-1 or simian/human immunodeficiency virus (SHIV) in humanized mice and macaques, respectively (Burton et al., 2012; Klein et al., 2013b; Mascola and Haynes, 2013). Moreover, combinations of bNAbs can also suppress established HIV-1 and SHIV infections (Barouch et al., 2013; Klein et al., 2012; Shingai et al., 2013). It is therefore believed that vaccines that elicit these antibodies would be protective against HIV-1.

Most of the bNAbs characterized to date target one of four major sites of vulnerability on HIV-1 Env: on gp120, the CD4-binding site, V1/V2, and the base of the V3 loop; and on gp41, the membrane-proximal external region (MPER) (Burton et al., 2012; Klein et al., 2013b; Mascola and Haynes, 2013). 8ANC195 is among a small group of bNAbs that does not appear to target any of these sites. Although only two of the B cells originally isolated from the 8ANC195 donor, an HIV-1 elite controller, belonged to the 8ANC195 clone, the antibodies produced by this clone complemented the neutralizing activity of antibodies produced by a more expanded B cell clone that targeted the CD4-binding site (Scheid et al., 2011).

8ANC195 is classified as a bNAb because it neutralized 66% of viruses in a diverse viral panel (Scheid et al., 2011). Like other anti-HIV-1 bNAbs (Klein et al., 2013a; Scheid et al., 2009a), 8ANC195 is highly somatically mutated, including insertions and deletions in the complementarity determining regions (CDRs) and framework regions (FWRs) of its heavy chain (HC) and light chain (LC). Although initial efforts to map the 8ANC195 epitope were unsuccessful (Scheid et al., 2011), computational analyses of neutralization data predicted that intact potential *N*-linked glycosylation sites (PNGSs) at positions 234_{gp120} and 276_{gp120} were essential for its activity (Chuang et al., 2013; West et al., 2013). These predictions were confirmed by evaluating the neutralization potency of 8ANC195 against mutant HIV-1 strains in vitro (Chuang et al., 2013; West et al., 2013) and in vivo (West et al., 2013). However, the precise 8ANC195 epitope on HIV-1 Env remained elusive.

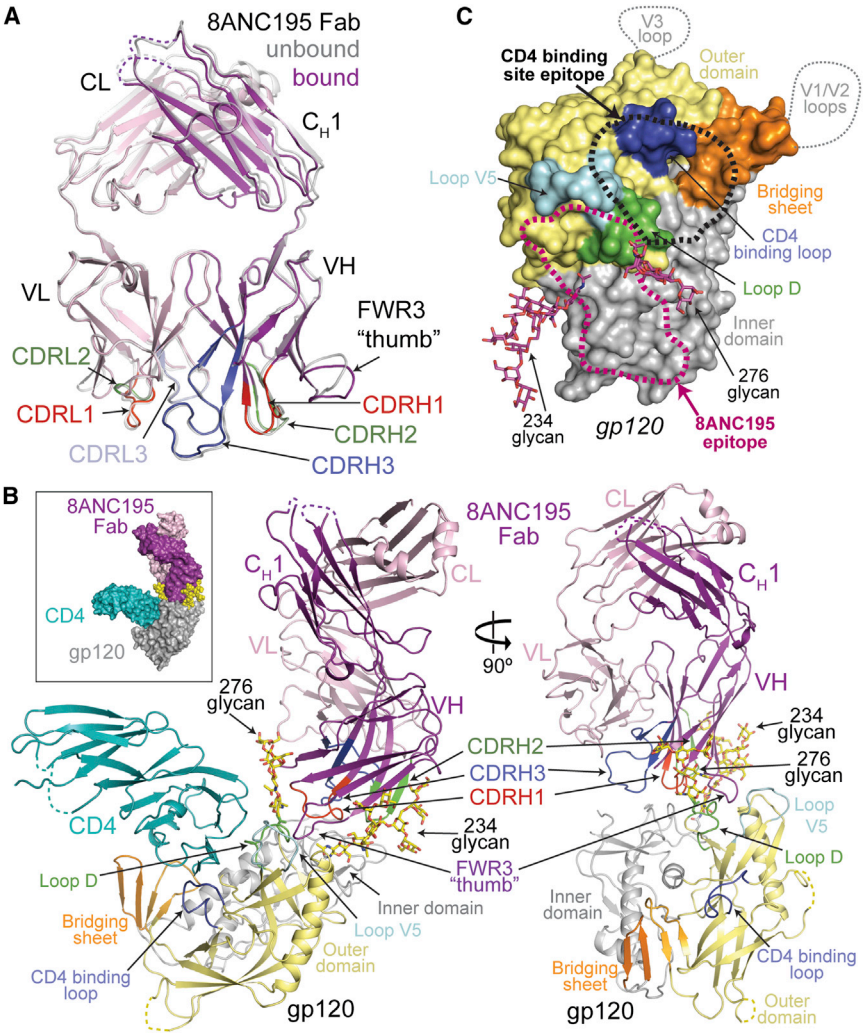

Figure 1. Crystal Structures of 8ANC195 Fab and 8ANC195/gp120/sCD4 Complex

(A) Superimposition of unbound (gray) and bound (HC, purple; LC, light pink) structures of 8ANC195 Fab shown as ribbon diagrams. CDR loops are highlighted (CDRH1/CDRL1 in red, CDRH2/CDRL2 in green, CDRH3 in dark blue, and CDRL3 in light blue), and a "thumb"-like loop formed by an insertion in FWR3 is indicated. Disordered loops are shown as dashed lines.

(B) Space-filling model (inset) and ribbon diagram of ternary complex of 8ANC195 (HC, purple; LC, light pink), sCD4 (teal), and 93TH057 gp120 core (inner domain, gray; outer domain, light yellow; bridging sheet, orange; loop D, green; loop V5, cyan; CD4-binding loop, blue). Ordered glycans attached to $Asn234_{gp120}$ and $Asn276_{gp120}$ are shown as yellow sticks (oxygens in red and nitrogens in blue). Fab CDR loops are colored as in (A). sCD4 was omitted from the right panel for clarity.

(C) Approximate locations of bNAb epitopes on a surface representation of the gp120 core. The epitopes of V3 and V1/V2 antibodies include regions of loops (dotted lines) not present in the gp120 core structure. CD4-binding site and 8ANC195 epitopes are outlined by black (CD4-binding site) and magenta (8ANC195) dots. Glycans included in the 8ANC195 epitope are shown in magenta. Subdomains of gp120 are colored as in (B).

See also Figure S1.

RESULTS

Crystal Structures of 8ANC195 Alone and in Complex with gp120 and CD4

To determine the epitope recognized by 8ANC195 and investigate its neutralization mechanism, we solved the crystal structures of the Fab fragment of 8ANC195 alone and complexed with an HIV-1 clade A/E 93TH057 gp120 core and CD4 domains 1–2 (sCD4) at 2.1 and 3.0 Å resolution, respectively (Figures 1A and 1B; Table S1). To reduce glycan heterogeneity, five PNGSs on the core gp120 were removed by mutation ($Asn88Gln_{gp120}$, $Asn289Gln_{gp120}$, $Asn334Gln_{gp120}$, $Asn392Gln_{gp120}$, and $Asn448Gln_{gp120}$), and the gp120 was expressed in human embryonic kidney 293S (HEK293S) $GnTI^{-/-}$ cells, which attach only high-mannose *N*-linked glycans to PNGSs, rather than a mixture of high-mannose, complex, and hybrid-type *N*-linked glycans (Binley et al., 2010; Dunlop et al., 2010).

Comparison of 8ANC195 Fab in its free versus gp120-bound state revealed high structural similarity (root mean square deviation of 0.7 Å for 236 Cα atoms of V_H-V_L) except for a 3.5 Å displacement of the loop connecting strands D and E in HC FWR3 (Figure 1A). The CDRH1 and CDRH3 loops were folded into hook-like tertiary structures in free and gp120-bound Fabs; therefore, the conformations were not induced upon binding to gp120 (Figures 1A, 2A, and 2B). The CDRH3 architecture differed from CDRH3s in other antibodies, including anti-HIV-1 antibodies with long CDR loops (Figure 2C). The CDRH1 loop conformation was stabilized by a hydrogen bond network among backbone atoms of CDRH1, burial of $Phe30_{HC}$, and hydrogen bonds with $Asp73_{HC}$ and $Thr97_{HC}$ (Figure 2A). CDRH3 had a complex tertiary structure in which residues 95_{HC}–$100c_{HC}$ formed a loop protruding ~10 Å from the antibody surface, and residues $100d_{HC}$–$100k_{HC}$ formed a β sheet subdomain that was stabilized by hydrophobic stacking between $His100f_{HC}$ and $Trp32_{LC}$ and a hydrogen bond between $Met100j_{HC}$ and $Gln89_{LC}$ (Figure 2B). The side chain of $Tyr92_{LC}$ hydrogen bonded with the $Gly100c_{HC}$ carbonyl oxygen, stabilizing a kink in the loop that formed the transition between these secondary structure elements (Figure 2B).

The complex structure showed independent binding of sCD4 and 8ANC195 Fab to distinct sites on gp120 (Figure 1B). sCD4 interacted with the gp120 core as in other sCD4-gp120 structures (Kwong et al., 1998) (Figure S1A); thus, its binding was not altered by the presence of the adjacent antibody, consistent with binding and neutralization experiments showing no effects of CD4 addition on 8ANC195 activity (Figures S1B and

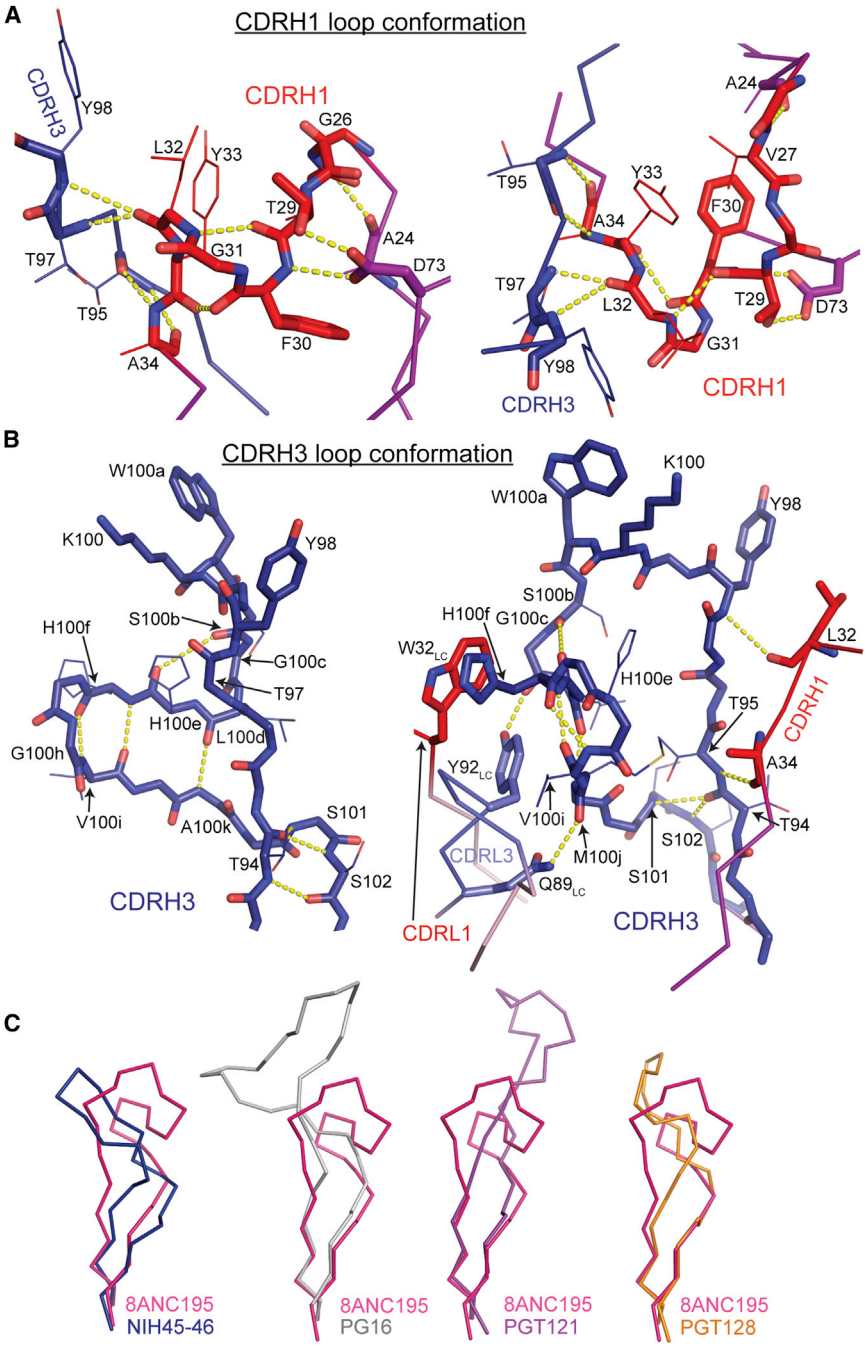

Figure 2. Conformations of 8ANC195 CDRH1 and CDRH3 Loops

(A) The hook-like conformation of CDRH1 (red) is stabilized by burial of the hydrophobic $Phe30_{HC}$ side chain and hydrogen bonds within CDRH1 and with CDRH3 (blue) and FWR1 and FWR3 residues ($Ala24_{HC}$ and $Asp73_{HC}$, respectively).

(B) The CDRH3 conformation (blue) consists of a protruding loop (residues 95_{HC}–$100c_{HC}$) and a small β sheet subdomain (residues $100d_{HC}$–$100k_{HC}$) stabilized by multiple hydrogen bonds within CDRH3 as well as with CDRH1 and CDRL3. A hydrogen bond between $Tyr92_{LC}$ and $Gly100c_{HC}$ stabilized the bifurcation of CDRH3 into its two subdomains. CDRH1 and CDRH3 loop backbone atoms are shown as sticks, and side chains of residues important for stabilizing the loop conformations are shown as sticks (involved in direct contacts) or lines (backbone involved in contacts). Other side chains ($Tyr98_{HC}$, $Lys100_{HC}$, and $Trp100a_{HC}$) are shown for clarity.

(C) Comparison of CDRH3 loops in 8ANC195 and other anti-HIV-1 bNAbs. CDRH3 residues corresponding to $8ANC195_{HC}$ residues 90–105 (pink) of NIH45-46 (blue; PDB 3U7Y), PG16 (gray; PDB 4DQO), PGT121 (purple; PDB 4FQC), and PGT128 (orange; PDB 3TYG) are shown as Cα traces.

S1C). sCD4 did, however, contribute to crystal packing (Figure S1D), which may explain why diffraction-quality crystals failed to grow in its absence. In the ternary complex structure, 8ANC195 bound to a gp120 region adjacent to the CD4-binding site, contacting mainly the gp120 inner domain, loops D and V5, and a small patch of the gp120 outer domain ($His352_{gp120}$–$Asn354_{gp120}$) (Figures 1B and 1C).

8ANC195 Fab bound gp120 core exclusively with its HC, using residues in FWRs and its three CDR loops to form an extensive interface (3,747 $Å^2$ total buried surface area; 1,347 $Å^2$ HC-gp120 protein contacts; 2,400 $Å^2$ HC-gp120 glycan contacts) (Figures 1B, 3, and S2; Table S2). A loop in $FWR3_{HC}$, consisting of somatically mutated residues and extended by a four-residue insertion, reached like a thumb into the pocket formed by loops D and V5 and outer-domain residues 352_{gp120}–358_{gp120} (Figures 1A, 1B, 3A, and S2B). Deletion of the FWR3 insertion that results in the protruding "$FWR3_{HC}$ thumb" abrogated neutralization activity of 8ANC195 (Figure S1E). CDRH1 and CDRH3 contacted the gp120 inner domain (Figures 3B and S2B), contributing to a 1,347 $Å^2$ interface between the 8ANC195 HC and gp120 protein residues. The CDRH1 and CDRH3 loop conformations, conserved in the free Fab (Figures 1A, 2A, and 2B), were necessary for binding gp120 because extending these loops would result in clashes with gp120. The resulting antibody-combining site was exquisitely suited to contacting portions of the inner domain of gp120 not targeted by other bNAbs (Figure 1C).

The 8ANC195 Fab also made extensive interfaces with glycans attached to $Asn234_{gp120}$ (buried surface area, 1,645 $Å^2$) and $Asn276_{gp120}$ (buried surface area, 755 $Å^2$), consistent with its dependence on these PNGSs for neutralization (Chuang et al., 2013; West et al., 2013). Together with CDRH2, somatically mutated FWR residues in strands B, C″, D, and E contributed to

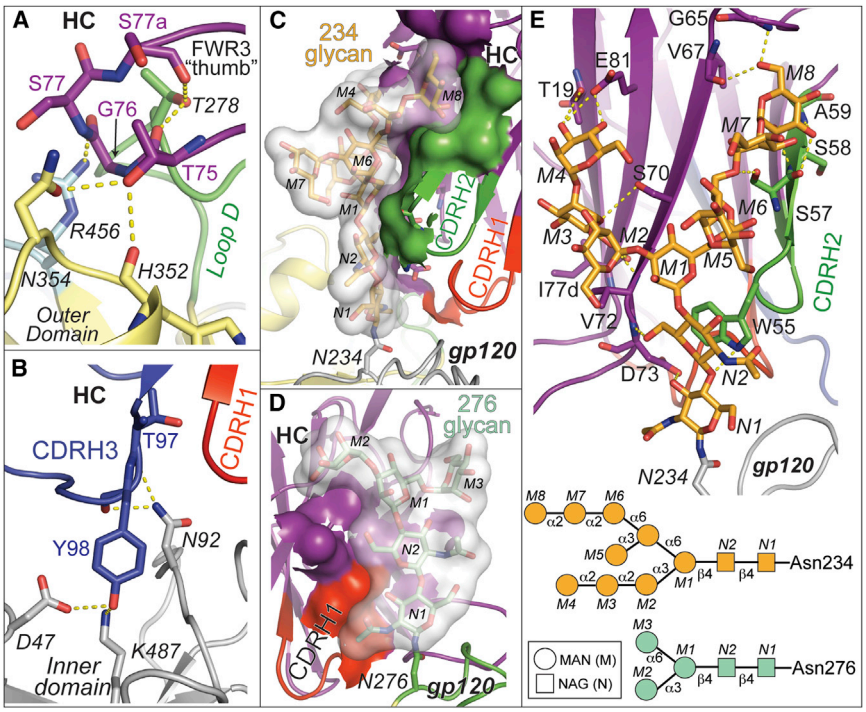

Figure 3. Contacts Made by 8ANC195 HC with gp120 Protein Residues and Glycans

Labels for gp120 protein and glycan residues are italicized. Hydrogen bonds are shown as dashed yellow lines.

(A) $FWR3_{HC}$ loop contacts with loop D (green), loop V5 (light blue), and outer-domain loop (yellow).

(B) 8ANC195 HC CDRH1 (red) and CDRH3 (blue) contacts with gp120 inner domain (gray).

(C) Buried surface area between the $Asn234_{gp120}$ glycan (transparent surface with glycan residues shown as sticks) and 8ANC195 (HC FWR residues in purple and CDRH2 in green). Antibody atoms buried by glycan interactions are shown as surfaces.

(D) Buried surface area between the Asn276 $glycan_{gp120}$ (transparent surface with glycan residues shown as sticks) and 8ANC195 (HC FWR residues in purple and CDRH1 in red). Antibody atoms buried by glycan interactions are shown as surfaces.

(E) Top: contacts made by 8ANC195 HC FWR residues (purple) and CDRH2 (green) with $Asn234_{gp120}$ glycan (orange). Glycan and protein residues involved in hydrogen bonds are shown as sticks. Bottom: schematic representations of ordered high-mannose glycans on $Asn234_{gp120}$ and Asn276 $_{gp120}$ (bottom).

See also Figure S2.

an extensive interface with the $Asn234_{gp120}$-associated *N*-glycan (usually high mannose in native HIV-1 Envs; Go et al., 2011) that involved ten sugar moieties, including specific interactions with terminal mannose residues (Figures 3C, 3E, and S2C–S2H). Although $Man_5GlcNAc_2$ glycans comprise the majority of *N*-glycans on gp120 proteins produced in $GnTI^{-/-}$ cells, $Man_{6\text{-}9}GlcNAc_2$ have also been found (Dunlop et al., 2010), and the D1,D3-$Man_8GlcNAc_2$ structure of the $Asn234_{gp120}$-associated *N*-glycan was verified by simulated annealing omit maps (Figures S3E and S3H). A two-residue deletion at the CDRH2–$FWR3_{HC}$ boundary compared to the germline sequence permitted these interactions because the longer loop would clash with inner-domain residue $Asn234_{gp120}$ and its neighbors. The $Asn276_{gp120}$ glycan (a complex-type *N*-glycan in native HIV-1 Envs [Binley et al., 2010; Go et al., 2011], but high mannose in the crystallized gp120) was wedged between 8ANC195 and sCD4, where it contacted FWR residues in strands A and B and the N-terminal portion of CDRH1, forming an interface involving only the core pentasaccharide common to both high-mannose and complex-type *N*-glycans (Figures 3D, S2F, and S2G). Recognition of the common core pentasaccharide has been suggested to be an adaptation evolved by glycan-dependent bNAbs such as PGT121 to recognize both complex-type and high-mannose glycans at a particular PNGS on Env (Mouquet et al., 2012). In the case of the 8ANC195 interaction with the $Asn276_{gp120}$ glycan, modeling indicates that the core fucose of a complex-type *N*-glycan could be accommodated by the antibody (Figure S3I); thus, 8ANC195 may also exhibit promiscuous recognition of certain *N*-glycans.

The 8ANC195 HC was bracketed by the $Asn234_{gp120}$ and $Asn276_{gp120}$ glycans in a manner analogous to interactions of HIV-1 antibodies that penetrate the Env glycan shield, such as PG16 (interactions with $Asn160_{gp120}$ and $Asn156_{gp120}$/$Asn173_{gp120}$ glycans) (Pancera et al., 2013), PGT128 (with $Asn301_{gp120}$ and $Asn332_{gp120}$ glycans) (Pejchal et al., 2011), and PGT121 (with $Asn332_{gp120}$ and $Asn137_{gp120}$ glycans) (Julien et al., 2013a, 2013b; Mouquet et al., 2012) (Figure 4). However, in contrast to these antibodies, 8ANC195 contacts with gp120 were made exclusively by its HC; indeed, 33% of 8ANC195 V_H domain residues not buried at the LC interface contacted gp120. In summary, the 8ANC195-gp120 structure demonstrated that 8ANC195 recognizes a previously undescribed epitope involving the $Asn234_{gp120}$ and $Asn276_{gp120}$ glycans, the gp120 inner domain, and loops D and V5, which would be adjacent to gp41 in Env trimer (Julien et al., 2013a; Lyumkis et al., 2013).

EM Reconstruction of 8ANC195 Bound to Soluble Env Trimer

To investigate portions of the 8ANC195 epitope beyond the gp120 core, including potential contacts with gp41, we used negative stain single-particle electron microscopy (EM) to determine the structure of 8ANC195 Fab bound to a soluble HIV-1 Env trimer with SOSIP mutations derived from strain BG505 (Figures 5A and S3) (Julien et al., 2013a; Lyumkis et al., 2013; Sanders et al., 2013). Independent docking of the BG505 Env trimer structure (Protein Data Bank [PDB] 4NCO) (Julien et al., 2013a) and 8ANC195 Fab resulted in a model wherein the Fab contacted both gp120 and gp41 within a single protomer (Figures 5A and S3). As expected from the lack of gp41 in the complex crystal structure and the low resolution of the EM structure, a small difference in Fab placement was observed between the two structures (Figures S3D and S3E). The EM model placed

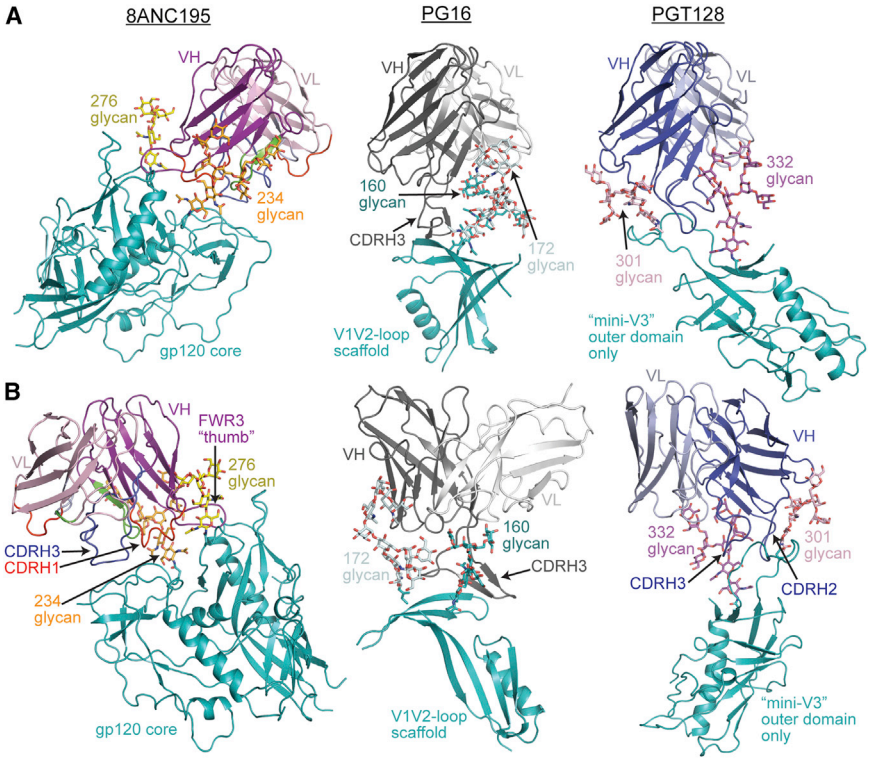

Figure 4. Comparison of Glycan-Dependent bNAbs

8ANC195 is bracketed by two glycans ($Asn234_{gp120}$ glycan in orange; $Asn276_{gp120}$ glycan in yellow) in the 8ANC195 Fab/gp120/sCD4 complex structure (left panels). For comparison, crystal structures of PG16 (gray, middle panels; PDB 4DQO) bound to a V1/V2 loop scaffold and PGT128 (blue, right panels; PDB 3TYG) bound to a V3 loop scaffold are shown with (A) the antibody HCs aligned to the 8ANC195 HC or (B) an alternative view showing their interactions with bracketing glycans (for PG16, $Asn160_{gp120}$ glycan is in teal, and $Asn172_{gp120}$ glycan is in light cyan; for PGT128, $Asn301_{gp120}$ glycan is in pink, and $Asn332_{gp120}$ glycan is in purple). The proteins are shown as ribbon diagrams and the glycans as stick representations.

the CDRL1, CDRL2, and portions of $FWR3_{LC}$ and CDRH3 in close proximity to the HR2 helix of gp41 (Figure 5B). Although gp41 residues were not definitively identified in the trimer crystal structure (Julien et al., 2013a), based on the assignment of the HR2 C terminus as $Gly664_{gp41}$ (Lyumkis et al., 2013), the kink in the HR2 helix was assigned as $Asn637_{gp41}$ (Figures 5B and S4), the asparagine of a highly conserved PNGS. This assignment was consistent with mapping of gp41 residues 651–664 to the end of a helix at the base of the Env trimer, as determined by difference mapping to determine the position of residue 650_{gp41} (Lyumkis et al., 2013). By counting backward from residue 650_{gp41}, the kink in the HR2 helix can be assigned as residue $Asn637_{gp41}$. In addition, although the glycan at $Asn637_{gp41}$ was not built into the model for the 4.7 Å crystal structure of the BG505.SOSIP trimer (Julien et al., 2013a), difference Fourier maps calculated using the PDB 4NCO structure factors showed electron density for the first GlcNAc of this glycan (Figure S3G). The 8ANC195-Env trimer EM model predicted that the $Asn637_{gp41}$-linked glycan and adjacent amino acid residues on HR2 interacted with 8ANC195 CDRH3, CDRL1, and CDRL2. Despite the predicted contacts with the $Asn637_{gp41}$-linked glycan, a mutant YU2 pseudovirus lacking the glycan ($Asn637_{gp41}Gln$) did not show decreased sensitivity to 8ANC195 (Table S3). However, the gp120 portion of the 8ANC195 epitope is so extensive that it could mask or compensate for contributions made by a smaller gp41 portion of the epitope. In addition, the effects of removing a glycan at an antibody-antigen interface can be unpredictable. For example, the VRC01-like bNAbs contact $Asn276_{gp120}$ on Env (Diskin et al., 2013), yet viral strains and mutants that do not contain the glycan can show increased, rather than decreased, sensitivity in neutralization assays (Li et al., 2011).

Light Chain Involvement in Neutralization of HIV-1 by 8ANC195

The EM reconstruction highlighted a potential role for 8ANC195 LC contacts to gp41. To assess LC contacts with trimeric Env, we tested chimeras consisting of the 8ANC195 HC paired with different LCs in neutralization and binding assays. The chimeras included a full germline LC, a mature LC with individual CDR loops reverted to their germline sequences or CDRL3 partially mutated to alanines, or the LC from the CD4-binding site antibody 3BNC117 (Figure 6A). As expected from the crystal structure in which all gp120 contacts were made by the 8ANC195 HC, the chimeras bound normally to full-length 93TH057 and YU2 gp120s (Figure 6B; Table S3); thus, changes in the LC did not disrupt the HC portion of the antibody-combining site.

In contrast to gp120 binding, neutralization potencies assayed against native Env spike trimers were decreased by changes in the 8ANC195 LC. For example, reverting CDRL1 and CDRL2 sequences to germline precursor sequences (changing 3 of 7 and 3 of 3 residues, respectively) almost completely abrogated neutralization of YU2, an 8ANC195-sensitive strain. Changes to CDRL3 led to a moderate reduction in neutralization potency, as did substituting the 3BNC117 LC for the cognate LC (Figure 6B; Table S3). A chimeric immunoglobulin G (IgG) with one of the most conservatively substituted LCs (Thr-Gly-Asn, mature CDRL1 containing a one-residue insertion, reverted to Ser-Ser, germline CDRL1) displayed unchanged binding to gp120, yet showed reductions in neutralization potency of up to 250-fold. Similarly, conservative changes in CDRL2 (Arg-Gly-Ala, the mature CDRL2, reverted to the germline Lys-Ala-Ser sequence) caused large reductions in neutralization potencies but had little effect on gp120 binding. Overall, the data showed differential sensitivities of the binding and neutralization assays to changes in the 8ANC195 LC that

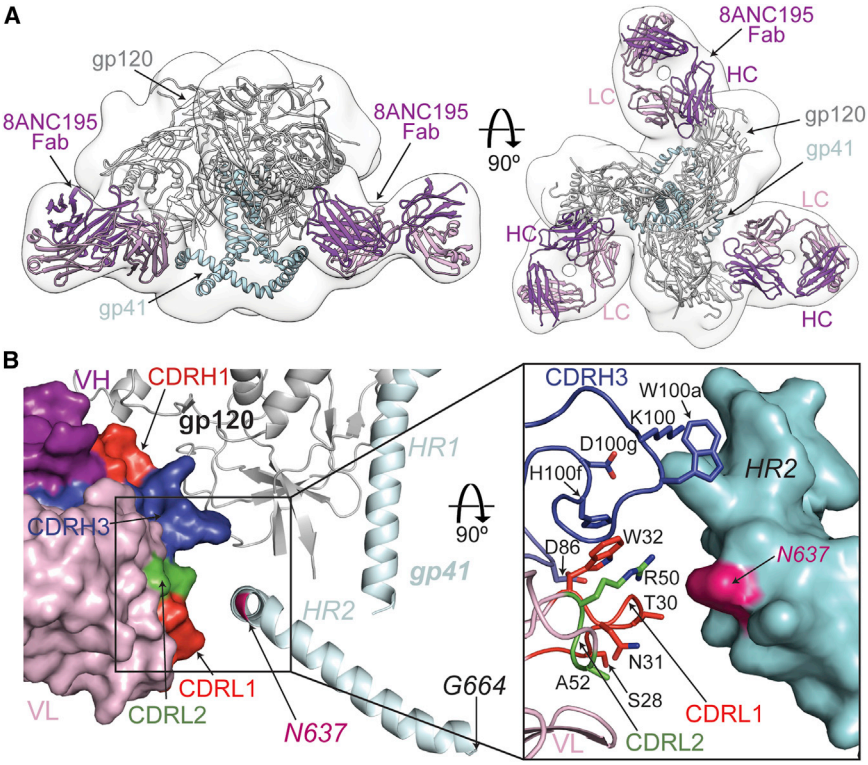

Figure 5. EM Reconstruction of 8ANC195/Env Trimer Complex and Model of 8ANC195 LC Interactions with gp41 HR2

(A) EM reconstruction of 8ANC195 Fab/BG505 SOSIP.664. Side (left) and top (right) views of EM density with the X-ray structures of BG505 SOSIP.664 (PDB 4NCO; gp120 in gray, and gp41 in light blue) and 8ANC195 Fab fit independently of gp140 coordinates to the EM density (purple). See also Figure S3.

(B) Close-up view of 8ANC195 LC/HR2 region of EM complex structure (Fab placement is independently placed as in A). In the left panel, 8ANC195 Fab is shown as a surface representation with highlights (CDRL1 in red, CDRL2 in green, CDRH1 in red, and CDRH3 in blue), and gp140 is shown as a ribbon diagram (gp120 in gray, and gp41 in light blue). The position of $Asn637_{gp41}$ (magenta) was deduced from the position of the C terminus of the SOSIP.664 trimer ($Gly664_{gp41}$). The right panel shows 8ANC195 HC and LC residues (sticks) positioned to contact HR2, which is shown as a surface representation calculated from HR2 coordinates in PDB 4NCO with presumptive side chains added to the poly-alanine coordinates.

See also Figure S4.

were distant from the gp120 surface, which supported the EM results suggesting that LC, and CDRL1 and CDRL2 in particular, contacted gp41.

Isolation of Clonal Members of the 8ANC195 Family

To further investigate Env recognition by 8ANC195, we isolated additional members of this antibody clone from the original donor by single-cell sorting using gp120 stabilized in the CD4-bound conformation (2CC core) as bait (Figure S5). Of 1,536 single 2CC core-binding B cells, 10 (0.7%) were clonally related to 8ANC195, and of these, only 4 differed slightly from the 2 previously described members (1–3 and 1–7 residue differences in the HCs and LCs, respectively) (Figure S5). Consistent with the limited sequence diversity, these antibodies exhibited similar potencies to 8ANC195 in neutralization assays against a panel of 15 Tier 2 viruses (Figure S5C; Table S4).

Reasoning that the 2CC core bait might fail to capture some 8ANC195 family members, we used clone-specific primers to amplify 8ANC195 variants from purified populations of CD19+ IgG+ memory B cells (Figure S6). We obtained 128 HC and 100 LC sequences that were clonally related to 8ANC195 and displayed greater sequence diversity than antibodies obtained using antigen-specific selection (Figure S6). Combinations of the 11 HC and 11 LC genes exhibiting greatest diversity were co-transfected in order to evaluate their neutralizing activity against a 15-member Tier 2 virus panel. Of 67 new antibodies, 3 (4.5%) were at least as broad and potent as 8ANC195 (Figure 6C; Table S5). One of these, $\gamma52_{HC}\kappa5_{LC}$, was 5-fold more potent than 8ANC195 (neutralized 12 of 15 viruses with a mean IC_{50} of 0.45 μg/ml as compared to 2.3 μg/ml for 8ANC195) (Table S5), a potency and breadth against this virus panel that was comparable to bNAbs that target nonoverlapping sites (Mouquet et al., 2012; Wu et al., 2010), such as VRC01 (neutralized 12 of 15 viruses with a 0.56 μg/ml mean IC_{50}), and more broad but less potent than 10-1074 (neutralized 6 of 15 viruses with a mean of 0.09 μg/ml).

The LC was critical to the activity of the more potent $\gamma52_{HC}$ $\kappa5_{LC}$ variant, as demonstrated by diminished neutralization potencies when $\kappa5_{LC}$ was swapped for either $\kappa3_{LC}$ or $\kappa11_{LC}$ (Figure 6C). The weaker neutralization could be explained by differences between $\kappa5_{LC}$ and $\kappa3_{LC}$ at solvent-exposed residues in CDRL2 (53_{LC} and 54_{LC}) and FWRL3 (64_{LC}), and a nearby buried residue (34_{LC}) that may affect the structural integrity of CDRL1. Modeling of YU2 gp41 residues into the Env trimer structure (Julien et al., 2013a) suggested that 8ANC195 positions 53_{LC} and 54_{LC} were adjacent to the $Asn637_{gp41}$ PNGS (Figures S4D and S7). The improved neutralizing activity of $\kappa5_{LC}$ compared with the other newly isolated LCs was associated with small side chains at positions 34_{LC} (Val), 53_{LC} (Ala), and 54_{LC} (Ala), whereas $\kappa3_{LC}$ or $\kappa11_{LC}$, which were less broadly neutralizing when paired with identical HCs, included bulkier and/or charged side chains that would clash with the nearby gp41 glycan. $\kappa5_{LC}$ was the only LC containing an $S64R_{LC}$ substitution, and this single change compared to the 8ANC195 LC may account for the 5-fold improved potency of $\gamma52_{HC}\kappa5_{LC}$. Residues in the immediate vicinity of $Asn637_{gp41}$ might also modify neutralization (a computational analysis of neutralization panel data using the Antibody Database program (West et al., 2013) suggested that $Glu632_{gp41}$ was associated with stronger neutralization).

A

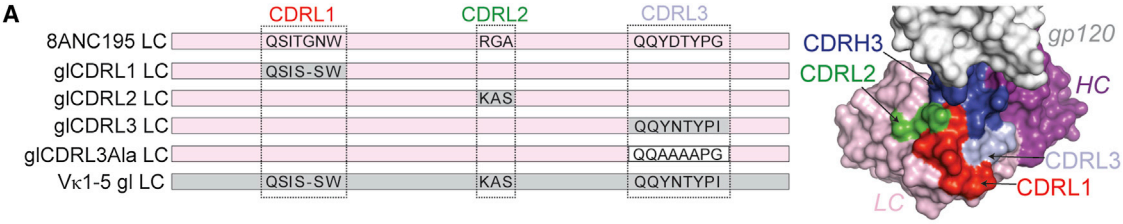

B

Antibody	K_D (fold change)		IC_{50} (fold change)					
	93TH057 gp120	YU2 gp120	YU2	Tro11	SF162	6535_3	SC4226618	PVO4
8ANC195 IgG	1	1	1	1	1	1	1	1
8ANC195 mHC/glLC	1.1	0.7	17	>250	43	21	12	22
8ANC195 glCDRL1	1.1	1.3	138	>250	218	57	140	>250
8ANC195 glCDRL2	1.2	1.5	16	62	147	31	99	187
8ANC195 glCDRL3	1.3	1.3	2	2	3	3	2	6
8ANC195 CDRL3Ala	ND	ND	97	ND	>250	>250	>250	>250
8ANC195HC/3BNC117LC	ND	ND	12	17	19	>250	32	ND

Fold change compared to 8ANC195 IgG: 1-5 6-20 21-100 >100

C

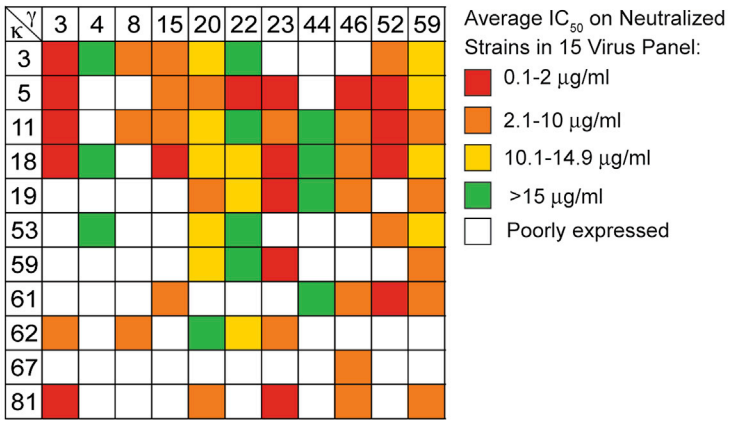

Figure 6. Effects of LC Sequence Changes on 8ANC195 Neutralization Potency

(A) Sequences of LC CDRs in constructs used with 8ANC195 HC to make chimeric IgGs (left) and location of CDRs on 8ANC195 structure (right). Sequences derived from the mature antibody are shown on a pink background; those derived from the germline precursor are shown on a gray background. The mutations introduced into CDRL3 in glCDRL3Ala are shown on a white background.

(B) Effects of changes in 8ANC195 LC on binding to 93TH057 and YU2 gp120s and neutralization of viral strains, expressed as fold changes over results for 8ANC195 IgG. *K*D and IC50 values for these experiments are shown in Table S3.

(C) Heatmap showing the expression and neutralization of randomly paired HCs and LCs from the bulk sort on a Tier 2 15-virus panel. Red squares represent average IC_{50} values on neutralized viral strains (arithmetic means) between 0.1 and 2 μg/ml, orange squares between 2.1 and 10 μg/ml, yellow squares between 10.1 and 14.9 μg/ml, and green squares above 15 μg/ml. White squares represent insufficient antibody expression.

See also Figures S5 and S6.

DISCUSSION

8ANC195 defines a site of HIV-1 Env vulnerability that includes gp120 glycans and portions of the gp120 inner domain not targeted by other bNAbs. A single-particle EM reconstruction, supported by light chain paratope analysis, suggested that the epitope spans gp120 and gp41 (Figure 7). As such, 8ANC195 represents a patient-derived anti-HIV-1 antibody that spans both subunits of the Env trimer. An antibody generated by phage display was reported to exhibit binding to gp120 as well as to a gp41-Fc fusion protein, but it was selected in vitro for these independent binding activities, and there was no evidence that it contacts both Env subunits simultaneously on a native Env trimer (Zhang et al., 2012). By contrast, our structural, mutagenesis, and neutralization results suggest that the 8ANC195 epitope spans both subunits in a native trimer. Rather than penetrating the glycan shield using only a single CDR loop, a strategy employed by antibodies such as PG9 and PGT128 (McLellan et al., 2011; Pejchal et al., 2011), 8ANC195 inserted its entire HC variable region into a gap in the shield to form a large interface, of which >50% involved contacts to gp120 glycans. The recognition of both Env subunits by 8ANC195 may facilitate neutralization by preventing conformational changes required for gp41-mediated fusion of the host cell and viral membranes.

8ANC195 was one of two family members of a rare B cell clone, and the original antibody was less potent than some bNAbs targeting the CD4-binding site (Scheid et al., 2011; Wu

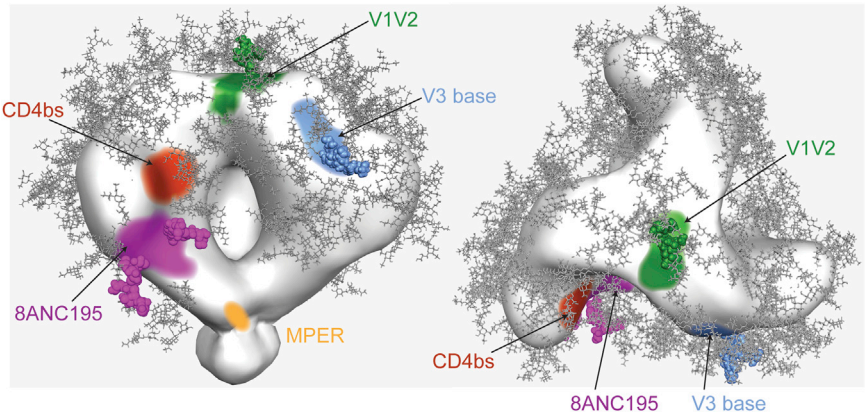

Figure 7. Locations of bNAb Epitopes on HIV-1 Env Trimer

EM density map of Env trimer including MPER (trimer map EMD-5019 [Liu et al., 2008]). showing approximate epitope locations for antibodies targeting the 8ANC195 epitope (purple with $Asn234_{gp120}$ and $Asn276_{gp120}$ glycans shown as spheres), CD4-binding site (red), V3 loop/$Asn332_{gp120}$ glycan (blue with $Asn332_{gp120}$ glycan shown as spheres), V1/V2 loop/$Asn160_{gp120}$ glycan (green with $Asn160_{gp120}$ glycan shown as spheres), and MPER (yellow).

et al., 2010) or V3 loop (Mouquet et al., 2012; Walker et al., 2011). Although it was not possible to obtain large numbers of 8ANC195 variants by standard single-cell cloning techniques (Scheid et al., 2009b), randomly combining HCs and LCs obtained from memory B cells without antigen-specific sorting demonstrated that the target of this antibody supported neutralization activity comparable to that against the most vulnerable sites on Env. Because 8ANC195 arose in an HIV-1-infected donor, it is possible for the human immune system to generate antibodies against this epitope, making it a valuable site to include on potential immunogens. Indeed, the footprint of this bNAb on gp120 primarily involves the inner domain, contrary to suggestions that efforts be made to focus the antibody response on the gp120 outer domain only (Nabel et al., 2011). Characterization of the potential gp120-gp41-bridging epitope highlights the importance of using properly folded gp120-gp41 Env trimers (Julien et al., 2013a; Lyumkis et al., 2013; Sanders et al., 2013) or building epitope scaffolds containing the gp120 outer and inner domains plus a portion of gp41 for immunogen design.

In addition to identifying vaccine targets, bNAbs could potentially be used therapeutically in established HIV-1 infections, especially bNAb combinations that limit escape by recognizing nonoverlapping epitopes (Barouch et al., 2013; Klein et al., 2012; Shingai et al., 2013). Potent variants of 8ANC195 may be particularly valuable in this respect because the epitope does not overlap with the targets of CD4-binding site, V1/V2 loop, V3 loop, or MPER antibodies.

EXPERIMENTAL PROCEDURES

Protein Expression and Purification

The antibodies used in this study were produced and purified as in previously described studies by Diskin et al. (2011). Briefly, 8ANC195 and its clonal variants, 3BNC60, and chimeric antibody (mature HC/various LC; γ/κ combinations of newly isolated 8ANC195 variants) IgGs were expressed by transiently transfecting HEK293-6E cells with vectors containing the appropriate HC and LC genes. Secreted IgGs were purified from cell supernatants using protein A affinity chromatography (GE Healthcare). For neutralization assays, IgGs were diluted to 1 mg/ml stocks in 20 mM Tris (pH 8.0), 150 mM sodium chloride (Tris-buffered saline [TBS] buffer). 8ANC195 Fab was expressed with a 6×-His tag on the C terminus of C_H1 as described for IgGs and purified using Ni^{2+}-NTA affinity chromatography (GE Healthcare) and Superdex 200 16/60 size exclusion chromatography (GE Healthcare).

A truncated gp120 from the HIV-1 strain 93TH057 containing mutations $Asn88Gln_{gp120}$, $Asn289Gln_{gp120}$, $Asn334Gln_{gp120}$, $Asn392Gln_{gp120}$, and $Asn448Gln_{gp120}$ was produced by transiently transfecting HEK293-S ($GnTI^{-/-}$) cells adapted for growth in suspension by the Caltech Protein Expression Center with a pTT5 vector encoding His-tagged gp120. Secreted gp120 was captured on Ni^{2+}-NTA resin (GE Healthcare) and further purified using Superdex 200 16/60 size exclusion chromatography.

Soluble CD4 domains 1 and 2 (sCD4) and $sCD4_{K75T}$ were produced as described previously by Diskin et al. (2010). Briefly, the pACgp67b vector encoding 6×-His-tagged sCD4 or $sCD4_{K75T}$ (residues 1–186 of mature CD4) was used to make infectious baculovirus particles using BaculoGold (BD Bioscience). Protein was expressed in Hi5 cells, captured on a Ni^{2+}-NTA column (GE Healthcare), and further purified using Superdex 200 16/60 size exclusion chromatography. To remove an *N*-linked glycan introduced by mutation in $sCD4_{K75T}$, the protein was treated with Endoglycosidase H (New England Biolabs) for 16 hr at 25°C and then purified by Superdex 200 16/60 size exclusion chromatography.

For complex crystallization trials, purified 8ANC195 Fab, 93TH057 gp120, and EndoH-treated $sCD4_{K75T}$ were incubated at a 1:1:1 molar ratio for 2 hr at 25°C. The complex was purified by Superdex 200 10/300 size exclusion chromatography (GE Healthcare) and the peak corresponding to 8ANC195 Fab/gp120/$sCD4_{K75T}$ complex concentrated to 16 mg/ml in TBS buffer. For crystallization of 8ANC195 Fab alone, the protein was concentrated to 20 mg/ml in TBS buffer.

Purified BG505 SOSIP trimers (Julien et al., 2013a, 2013b; Sanders et al., 2013) for EM studies were the gift of Dr. John P. Moore (Weill Cornell Medical College).

Crystallization

Crystals of 8ANC195 Fab (space group $P4_12_12$, a = 66.5 Å, b = 66.5 Å, and c = 219.0 Å; one molecule per asymmetric unit) were obtained upon mixing a protein solution at 11 mg/ml with 0.1 M HEPES (pH 7), 20% PEG 6,000, and 10 mM zinc chloride at 20°C. Crystals were briefly soaked in mother liquor solution supplemented with 20% ethylene glycol before flash cooling in liquid nitrogen. Crystals of the 8ANC195 Fab/93TH057 gp120/$sCD4_{K75T}$ complex (space group $P2_12_12_1$, a = 66.5 Å, b = 132.5 Å, and c = 142.8 Å; one molecule per asymmetric unit) were obtained upon mixing a protein solution at 16 mg/ml with 14% polyethylene glycol 3,350, 0.1 M HEPES (pH 7.3), and 2% benzamidine HCl at 20°C. Crystals were briefly soaked in mother liquor solution supplemented with 30% ethylene glycol before flash cooling in liquid nitrogen.

Crystallographic Data Collection, Structure Determination, and Refinement

X-ray diffraction data for 8ANC195 Fab crystals were collected at the Argonne National Laboratory Advanced Photon Source (APS) beamline 23-ID-D using a MAR 300 CCD detector. X-ray diffraction data for 8ANC195 Fab/93TH057 gp120/$sCD4_{K75T}$ complex crystals were collected at the Stanford Synchrotron Radiation Lightsource beamline 12-2 using a Pilatus 6M pixel detector (Dectris). The data were indexed, integrated, and scaled using XDS (Kabsch, 2010). The 8ANC195 Fab structure was solved by molecular replacement and refined

to 2.13 Å resolution using an iterative approach involving refinement and verification of model accuracy with simulated annealing composite omit maps using the PHENIX crystallography package (Adams et al., 2010), and manually fitting models into electron density maps using Coot (Emsley and Cowtan, 2004). The final model (R_{work}, 20.2%; R_{free}, 24.2%) includes 3,321 protein atoms, 15 ligand atoms, and 178 water molecules (Table S1). Of the residues, 99.54%, 0.46%, and 0.0% were in the favored, allowed, and disallowed regions, respectively, of the Ramachandran plot. Disordered residues that were not included in the model include residues 127–134 and 214–219 and the 6×-His tag of the 8ANC195 HC and residues 213–214 of the LC. The 8ANC195 Fab/93TH057 gp120/$sCD4_{K75T}$ complex structure was solved by molecular replacement and refined to 3.0 Å resolution as described for the Fab structure. In addition to considering I/σ_I and completeness of the highest-resolution shell (2.1% and 99.9%, respectively), we used the $CC_{1/2}$ statistic (Karplus and Diederichs, 2012) (correlation coefficient between two random halves of the data set where $CC_{1/2}$ >10%) to determine the high-resolution cutoff for our data. PHENIX (Adams et al., 2010) was used to compute $CC_{1/2}$ (85.4% for the highest-resolution shell and 99.8% for the entire data set), supporting our high-resolution cutoff determination. To prevent phase bias, no glycan residues were present during initial stages of refinement. Glycans were built manually in Coot (Emsley and Cowtan, 2004) into simulated annealing composite omit maps calculated using PHENIX (Adams et al., 2010) throughout the refinement process. The final model (R_{work}, 23.5%; R_{free}, 27.2%) includes 7,195 protein atoms and 408 atoms of carbohydrates and ligands (Table S1). Of the residues, 96.92%, 3.08%, and 0.0% were in the favored, allowed, and disallowed regions, respectively, of the Ramachandran plot. Disordered residues that were not included in the model include residues 126–135, 185–194, and 214–219 and the 6×-His tag of the 8ANC195 HC, residues 212–214 of the LC, residues 125–197 (V1/V2 substitution), 302–324 (V3 substitution), residues 396–408 (a total of 6 residues from V4), residues 492–494 and the 6×-His tag of 93TH057 gp120 and residues 106–111, 150–152, and 178–186, and the 6×-His tag of $sCD4_{K75T}$.

Buried surface areas were calculated using PDBePISA (Krissinel and Henrick, 2007) and a 1.4 Å probe. Superimposition calculations were done, and molecular representations were generated using PyMOL (Schrödinger, 2011). Pairwise Cα alignments were performed using PDBeFold (Krissinel and Henrick, 2004).

ELISAs

High-binding 96-well ELISA plates (Costar) were coated overnight with 5 μg/well of purified gp120 in 100 mM sodium carbonate (pH 9.6). After washing with TBS containing 0.05% Tween 20, the plates were blocked for 2 hr with 1% BSA, 0.05% Tween-TBS (blocking buffer), and then incubated for 2 hr with 8ANC195 IgG (1 μg/ml) mixed with 1:2 serially diluted solutions of potential antibody competitors (sCD4, J3 VHH, 3BNC60 Fab, and NIH45-46 Fab) in blocking buffer (competitor concentrations ranged from 5 to 320 μg/ml). After washing with TBS containing 0.05% Tween 20, the plates were incubated with horseradish peroxidase (HRP)-conjugated goat anti-human IgG antibodies (Jackson ImmunoResearch) (at 0.8 μg/ml in blocking buffer) for 1 hr. The ELISAs were developed by addition of HRP chromogenic substrate (TMB solution; BioLegend), and the color development was stopped by addition of 10% sulfuric acid. Experiments were performed in duplicate.

Surface Plasmon Resonance

Experiments were performed using a Biacore T100 (Biacore) using a standard single-cycle kinetics method. YU2 and 93TH057 gp120 proteins were primary amine coupled on CM5 chips (Biacore) at a coupling density of 1,000 RUs, and one flow cell was mock coupled using HBS-EP+ buffer. 8ANC195 and chimeric IgGs were injected over flow cells at increasing concentrations (62.5–1,000 nM), at flow rates of 20 μl/min with five consecutive cycles of 2 min association/1 min dissociation and a final 10 min dissociation phase. Flow cells were regenerated with three pulses of 10 mM glycine (pH 2.5). Apparent binding constants (K_D [M]) were calculated from single-cycle kinetic analyses after subtraction of backgrounds using a 1:1-binding model without a bulk reflective index (RI) correction (Biacore T100 Evaluation software). Binding constants for bivalent IgGs are referred to as "apparent" affinities to emphasize that the K_D values include potential avidity effects.

Neutralization Assays

A TZM-bl/pseudovirus neutralization assay was used to evaluate the neutralization potencies of the antibodies as described (Montefiori, 2005). Pseudoviruses were generated by cotransfection of HEK293T cells with an Env expression plasmid and a replication-defective backbone plasmid. Neutralization assays were preformed in-house for evaluating 8ANC195 LC chimeras (Table S3; Figure 4B) and by the Collaboration for AIDS Vaccine Discovery core neutralization facility for testing the newly isolated 8ANC195 clonal variants (Tables S4 and S5; Figures S5 and S6). Some of the in-house data were derived from neutralization assays that were dispensed automatically by a Freedom EVO (Tecan) liquid handler (IC_{50} values derived from manual and robotic assays agreed to within 2- to 4-fold). In all cases, neutralization was monitored by the reduction of a Tat-induced reporter gene (luciferase) in the presence of a 3- or 5-fold antibody dilution series (each concentration run in duplicate or triplicate) after a single round of pseudovirus infection in the TZM-bl cell line (Montefiori, 2005). Nonlinear regression analysis was used to calculate the concentrations at which half-maximal inhibition was observed (IC_{50} values).

Negative-Stain EM

The BG505 SOSIP.664/8ANC195 Fab complex and grids were prepared as described previously by Kong et al. (2013). The data were collected on an FEI Tecnai T12 electron microscope coupled with a Tietz TemCam-F416 4k x 4k CMOS camera using the Leginon interface (Suloway et al., 2005). Images were collected in 10° increments from 0° to −40° using a defocus range of 0.6–0.9 μm at a magnification of 52,000×, resulting in a pixel size of 2.05 Å at the specimen plane. Particles were selected using DoG Picker (Voss et al., 2009) within the Appion software package (Lander et al., 2009) and sorted from reference-free 2D class averages using the SPARX package (Penczek et al., 1992). An initial model was generated by common lines from class averages using the EMAN2 package (Tang et al., 2007) and was refined using 11,637 unbinned particles. The refinement was carried out using the SPARX package (Penczek et al., 1994) with C3 symmetry applied. The resulting resolution at a 0.5 Fourier shell correlation (FSC) cutoff was 18.7 Å (Figures S3B and S3C). Molecular representations were generated using Chimera (Pettersen et al., 2004).

Human Samples

Human samples were collected after signed informed consent in accordance with institutional review board-approved protocols by all participating institutions. Patient 8 was selected from a cohort of elite controllers that was followed at the Ragon Institute in Boston.

Isolation of 8ANC195 Variants

Single-cell clonal variants of 8ANC195 were isolated by 2CC core-specific single-cell sorting, followed by reverse transcription and immunoglobulin gene amplification as described previously (Scheid et al., 2011). Immunoglobulin genes were cloned into HC and LC expression vectors and cotransfected for IgG production as described previously by Tiller et al. (2008). IgG+ CD19+ memory B cells were bulk sorted on a FACSAria III cell sorter (BD Biosciences). Bulk mRNA was extracted using TRIzol (Invitrogen) and reverse transcribed as previously described (Scheid et al., 2011). 8ANC195-related HC and LC genes were PCR amplified using clone-specific primers. Amplification products were gel purified and cloned into TOPO TA sequencing vectors (Invitrogen) and expression vectors as described previously by Tiller et al. (2008).

Phylogenetic Tree and Alignment Assembly

Phylogenetic trees were assembled using Geneious Neighbor-Joining Tree Software. Sequence alignments were performed using DNASTAR Clustal W alignment software.

Computational Analysis

The program Antibody Database (West et al., 2013) was used to analyze 8ANC195 neutralization panel data from Scheid et al. (2011) and (Chuang et al. (2013). This method attempts to model the variation in neutralization potency across strains based on a sum of terms ("rules") corresponding to

specific residues or PNGS positions. With the free residual option deselected, the analysis finds a rule corresponding to ~3-fold better 8ANC195 neutralization for strains with $Glu632_{gp41}$. This correlation appears to hold across clades based on neutralization data for strains having the most favorable glycosylation pattern (PNGS at 234_{gp120} and 276_{gp120}, and not at 230_{gp120}) (West et al., 2013). For all clades, the residue at 632_{gp41} versus geometric mean IC_{50} values for 8ANC195 on strains with the most favorable glycosylation pattern was as follows: Glu, 0.43 μg/m (n = 53) versus Asp, 1.31 μg/m (n = 51). For separate clades, the correlations were Clade A: Glu, 0.47 μg/ml (n = 3); Asp, 1.30 μg/ml (n = 24); Clade B: Glu, 0.18 μg/ml (n = 15); Asp, 0.72 μg/ml (n = 6); and Clade C: Glu, 0.32 μg/ml (n = 2); Asp, 1.31 μg/ml (n = 20).

ACCESSION NUMBERS

Crystallographic atomic coordinates and structure factors have been deposited in the PDB (http://www.pdb.org) for the 8ANC195 Fab (4P9M) and 8ANC195 Fab-gp120-CD4 complex (4P9H) structures. The EM reconstruction has been deposited in the Electron Microscopy Data Bank (http://www.ebi.ac.uk/pdbe/emdb) (EMD-2625).

SUPPLEMENTAL INFORMATION

Supplemental Information includes Supplemental Experimental Procedures, seven figures, and five tables and can be found with this article online at http://dx.doi.org/10.1016/j.celrep.2014.04.001.

AUTHOR CONTRIBUTIONS

L.S. solved and analyzed crystal structures, performed and analyzed binding studies, and analyzed antibody mutant data. J.F.S. isolated 8ANC195 variants and analyzed neutralization assays. JH.L. solved and analyzed EM structure. A.P.W. performed computational analysis. C.C. performed binding assays. H.G. expressed and purified proteins. P.N.P.G., R.M., and M.S.S. performed and analyzed neutralization assays. L.S., J.F.S., JH.L., A.B.W., M.C.N., and P.J.B. analyzed data and wrote the manuscript.

ACKNOWLEDGMENTS

This research was supported by the National Institute of Allergy and Infectious Diseases of the National Institutes of Health Grants HIVRAD P01 AI100148 (to P.J.B. and M.C.N.) and HIVRAD P01 AI082362 (to A.B.W.) (the content is solely the responsibility of the authors and does not necessarily represent the official views of the National Institutes of Health); the Bill and Melinda Gates Foundation (Collaboration for AIDS Vaccine Discovery Grants 1040753 [to P.J.B.] and 38619s [to M.C.N.] and Comprehensive Antibody-Vaccine Immune Monitoring Consortium Grant 1032144 [to M.S.S.]); NIH Center for HIV/AID Vaccine Immunology and Immunogen Discovery 1UM1 AI100663-01 (to M.C.N.); American Cancer Society Grant PF-13-076-01-MPC (to L.S.); a Dissertation Fellowship from the California HIV/AIDS Research Program (to JH.L); and the Molecular Observatory at Caltech supported by the Gordon and Betty Moore Foundation. The EM work was conducted at the National Resource for Automated Molecular Microscopy at The Scripps Research Institute, which is supported by the Biomedical Technology Research Center program (GM103310) of the National Institute of General Medical Sciences. We thank John P. Moore and Albert Cupo (Weill Cornell Medical College) for purified SOSIP trimers, Anna Gazumyan and Cassie Liu (Rockefeller University) for help with antibody expression, Brittany Lewis (Cornell Medical School) for help with cloning of 8ANC195 variants, and the Caltech Protein Expression Center for producing antibody and gp120 proteins, generation of suspension-adapted HEK293-S cells, and use of the Biacore T100. Operations at the Stanford Synchrotron Radiation Lightsource are supported by the US Department of Energy and the National Institutes of Health. We thank the beamline staff at the Advanced Photon Source GM/CA-CAT for use and support for beamline 23ID-D. M.C.N. and P.J.B. are Howard Hughes Medical Institute investigators.

Received: March 4, 2014
Revised: April 1, 2014
Accepted: April 4, 2014
Published: April 24, 2014

REFERENCES

Adams, P.D., Afonine, P.V., Bunkóczi, G., Chen, V.B., Davis, I.W., Echols, N., Headd, J.J., Hung, L.W., Kapral, G.J., Grosse-Kunstleve, R.W., et al. (2010). PHENIX: a comprehensive Python-based system for macromolecular structure solution. Acta Crystallogr. D Biol. Crystallogr. *66*, 213–221.

Barouch, D.H., Whitney, J.B., Moldt, B., Klein, F., Oliveira, T.Y., Liu, J., Stephenson, K.E., Chang, H.W., Shekhar, K., Gupta, S., et al. (2013). Therapeutic efficacy of potent neutralizing HIV-1-specific monoclonal antibodies in SHIV-infected rhesus monkeys. Nature *503*, 224–228.

Binley, J.M., Ban, Y.E., Crooks, E.T., Eggink, D., Osawa, K., Schief, W.R., and Sanders, R.W. (2010). Role of complex carbohydrates in human immunodeficiency virus type 1 infection and resistance to antibody neutralization. J. Virol. *84*, 5637–5655.

Burton, D.R., Poignard, P., Stanfield, R.L., and Wilson, I.A. (2012). Broadly neutralizing antibodies present new prospects to counter highly antigenically diverse viruses. Science *337*, 183–186.

Chuang, G.Y., Acharya, P., Schmidt, S.D., Yang, Y., Louder, M.K., Zhou, T., Kwon, Y.D., Pancera, M., Bailer, R.T., Doria-Rose, N.A., et al. (2013). Residue-level prediction of HIV-1 antibody epitopes based on neutralization of diverse viral strains. J. Virol. *87*, 10047–10058.

Diskin, R., Marcovecchio, P.M., and Bjorkman, P.J. (2010). Structure of a clade C HIV-1 gp120 bound to CD4 and CD4-induced antibody reveals anti-CD4 polyreactivity. Nat. Struct. Mol. Biol. *17*, 608–613.

Diskin, R., Scheid, J.F., Marcovecchio, P.M., West, A.P., Jr., Klein, F., Gao, H., Gnanapragasam, P.N., Abadir, A., Seaman, M.S., Nussenzweig, M.C., and Bjorkman, P.J. (2011). Increasing the potency and breadth of an HIV antibody by using structure-based rational design. Science *334*, 1289–1293.

Diskin, R., Klein, F., Horwitz, J.A., Halper-Stromberg, A., Sather, D.N., Marcovecchio, P.M., Lee, T., West, A.P., Jr., Gao, H., Seaman, M.S., et al. (2013). Restricting HIV-1 pathways for escape using rationally designed anti-HIV-1 antibodies. J. Exp. Med. *210*, 1235–1249.

Dunlop, D.C., Bonomelli, C., Mansab, F., Vasiljevic, S., Doores, K.J., Wormald, M.R., Palma, A.S., Feizi, T., Harvey, D.J., Dwek, R.A., et al. (2010). Polysaccharide mimicry of the epitope of the broadly neutralizing anti-HIV antibody, 2G12, induces enhanced antibody responses to self oligomannose glycans. Glycobiology *20*, 812–823.

Emsley, P., and Cowtan, K. (2004). Coot: model-building tools for molecular graphics. Acta Crystallogr. D Biol. Crystallogr. *60*, 2126–2132.

Go, E.P., Hewawasam, G., Liao, H.X., Chen, H., Ping, L.H., Anderson, J.A., Hua, D.C., Haynes, B.F., and Desaire, H. (2011). Characterization of glycosylation profiles of HIV-1 transmitted/founder envelopes by mass spectrometry. J. Virol. *85*, 8270–8284.

Julien, J.P., Cupo, A., Sok, D., Stanfield, R.L., Lyumkis, D., Deller, M.C., Klasse, P.J., Burton, D.R., Sanders, R.W., Moore, J.P., et al. (2013a). Crystal structure of a soluble cleaved HIV-1 envelope trimer. Science *342*, 1477–1483.

Julien, J.P., Sok, D., Khayat, R., Lee, J.H., Doores, K.J., Walker, L.M., Ramos, A., Diwanji, D.C., Pejchal, R., Cupo, A., et al. (2013b). Broadly neutralizing antibody PGT121 allosterically modulates CD4 binding via recognition of the HIV-1 gp120 V3 base and multiple surrounding glycans. PLoS Pathog. *9*, e1003342.

Kabsch, W. (2010). Integration, scaling, space-group assignment and post-refinement. Acta Crystallogr. D Biol. Crystallogr. *66*, 133–144.

Karplus, P.A., and Diederichs, K. (2012). Linking crystallographic model and data quality. Science *336*, 1030–1033.

Klein, F., Halper-Stromberg, A., Horwitz, J.A., Gruell, H., Scheid, J.F., Bournazos, S., Mouquet, H., Spatz, L.A., Diskin, R., Abadir, A., et al. (2012). HIV therapy by a combination of broadly neutralizing antibodies in humanized mice. Nature *492*, 118–122.

Klein, F., Diskin, R., Scheid, J.F., Gaebler, C., Mouquet, H., Georgiev, I.S., Pancera, M., Zhou, T., Incesu, R.B., Fu, B.Z., et al. (2013a). Somatic mutations of the immunoglobulin framework are generally required for broad and potent HIV-1 neutralization. Cell *153*, 126–138.

Klein, F., Mouquet, H., Dosenovic, P., Scheid, J.F., Scharf, L., and Nussenzweig, M.C. (2013b). Antibodies in HIV-1 vaccine development and therapy. Science *341*, 1199–1204.

Kong, L., Lee, J.H., Doores, K.J., Murin, C.D., Julien, J.P., McBride, R., Liu, Y., Marozsan, A., Cupo, A., Klasse, P.J., et al. (2013). Supersite of immune vulnerability on the glycosylated face of HIV-1 envelope glycoprotein gp120. Nat. Struct. Mol. Biol. *20*, 796–803.

Krissinel, E., and Henrick, K. (2004). Secondary-structure matching (SSM), a new tool for fast protein structure alignment in three dimensions. Acta Crystallogr. D Biol. Crystallogr. *60*, 2256–2268.

Krissinel, E., and Henrick, K. (2007). Inference of macromolecular assemblies from crystalline state. J. Mol. Biol. *372*, 774–797.

Kwong, P.D., Wyatt, R., Robinson, J., Sweet, R.W., Sodroski, J., and Hendrickson, W.A. (1998). Structure of an HIV gp120 envelope glycoprotein in complex with the CD4 receptor and a neutralizing human antibody. Nature *393*, 648–659.

Lander, G.C., Stagg, S.M., Voss, N.R., Cheng, A., Fellmann, D., Pulokas, J., Yoshioka, C., Irving, C., Mulder, A., Lau, P.W., et al. (2009). Appion: an integrated, database-driven pipeline to facilitate EM image processing. J. Struct. Biol. *166*, 95–102.

Li, Y., O'Dell, S., Walker, L.M., Wu, X., Guenaga, J., Feng, Y., Schmidt, S.D., McKee, K., Louder, M.K., Ledgerwood, J.E., et al. (2011). Mechanism of neutralization by the broadly neutralizing HIV-1 monoclonal antibody VRC01. J. Virol. *85*, 8954–8967.

Liu, J., Bartesaghi, A., Borgnia, M.J., Sapiro, G., and Subramaniam, S. (2008). Molecular architecture of native HIV-1 gp120 trimers. Nature *455*, 109–113.

Lyumkis, D., Julien, J.P., de Val, N., Cupo, A., Potter, C.S., Klasse, P.J., Burton, D.R., Sanders, R.W., Moore, J.P., Carragher, B., et al. (2013). Cryo-EM structure of a fully glycosylated soluble cleaved HIV-1 envelope trimer. Science *342*, 1484–1490.

Mascola, J.R., and Haynes, B.F. (2013). HIV-1 neutralizing antibodies: understanding nature's pathways. Immunol. Rev. *254*, 225–244.

McLellan, J.S., Pancera, M., Carrico, C., Gorman, J., Julien, J.P., Khayat, R., Louder, R., Pejchal, R., Sastry, M., Dai, K., et al. (2011). Structure of HIV-1 gp120 V1/V2 domain with broadly neutralizing antibody PG9. Nature *480*, 336–343.

Montefiori, D.C. (2005). Evaluating neutralizing antibodies against HIV, SIV, and SHIV in luciferase reporter gene assays. Curr. Protoc. Immunol., Chapter 12, Unit 12 11.

Mouquet, H., Scharf, L., Euler, Z., Liu, Y., Eden, C., Scheid, J.F., Halper-Stromberg, A., Gnanapragasam, P.N., Spencer, D.I., Seaman, M.S., et al. (2012). Complex-type N-glycan recognition by potent broadly neutralizing HIV antibodies. Proc. Natl. Acad. Sci. USA *109*, E3268–E3277.

Nabel, G., Kwong, P., and Mascola, J. (2011). Progress in the rational design of an AIDS vaccine. Philos. Trans. R. Soc. Lond. B Biol. Sci. *366*, 2759–2765.

Pancera, M., Shahzad-Ul-Hussan, S., Doria-Rose, N.A., McLellan, J.S., Bailer, R.T., Dai, K., Loesgen, S., Louder, M.K., Staupe, R.P., Yang, Y., et al. (2013). Structural basis for diverse N-glycan recognition by HIV-1-neutralizing V1-V2-directed antibody PG16. Nat. Struct. Mol. Biol. *20*, 804–813.

Pejchal, R., Doores, K.J., Walker, L.M., Khayat, R., Huang, P.S., Wang, S.K., Stanfield, R.L., Julien, J.P., Ramos, A., Crispin, M., et al. (2011). A potent and broad neutralizing antibody recognizes and penetrates the HIV glycan shield. Science *334*, 1097–1103.

Penczek, P., Radermacher, M., and Frank, J. (1992). Three-dimensional reconstruction of single particles embedded in ice. Ultramicroscopy *40*, 33–53.

Penczek, P.A., Grassucci, R.A., and Frank, J. (1994). The ribosome at improved resolution: new techniques for merging and orientation refinement in 3D cryo-electron microscopy of biological particles. Ultramicroscopy *53*, 251–270.

Pettersen, E.F., Goddard, T.D., Huang, C.C., Couch, G.S., Greenblatt, D.M., Meng, E.C., and Ferrin, T.E. (2004). UCSF Chimera—a visualization system for exploratory research and analysis. J. Comput. Chem. *25*, 1605–1612.

Sanders, R.W., Derking, R., Cupo, A., Julien, J.P., Yasmeen, A., de Val, N., Kim, H.J., Blattner, C., de la Peña, A.T., Korzun, J., et al. (2013). A next-generation cleaved, soluble HIV-1 Env Trimer, BG505 SOSIP.664 gp140, expresses multiple epitopes for broadly neutralizing but not non-neutralizing antibodies. PLoS Pathog. *9*, e1003618.

Scheid, J.F., Mouquet, H., Feldhahn, N., Seaman, M.S., Velinzon, K., Pietzsch, J., Ott, R.G., Anthony, R.M., Zebroski, H., Hurley, A., et al. (2009a). Broad diversity of neutralizing antibodies isolated from memory B cells in HIV-infected individuals. Nature *458*, 636–640.

Scheid, J.F., Mouquet, H., Feldhahn, N., Walker, B.D., Pereyra, F., Cutrell, E., Seaman, M.S., Mascola, J.R., Wyatt, R.T., Wardemann, H., and Nussenzweig, M.C. (2009b). A method for identification of HIV gp140 binding memory B cells in human blood. J. Immunol. Methods *343*, 65–67.

Scheid, J.F., Mouquet, H., Ueberheide, B., Diskin, R., Klein, F., Oliveira, T.Y., Pietzsch, J., Fenyo, D., Abadir, A., Velinzon, K., et al. (2011). Sequence and structural convergence of broad and potent HIV antibodies that mimic CD4 binding. Science *333*, 1633–1637.

Schrödinger, L. (2011). The PyMOL Molecular Graphics System, Version 1.5 (Schrödinger, LLC).

Shingai, M., Nishimura, Y., Klein, F., Mouquet, H., Donau, O.K., Plishka, R., Buckler-White, A., Seaman, M., Piatak, M., Jr., Lifson, J.D., et al. (2013). Antibody-mediated immunotherapy of macaques chronically infected with SHIV suppresses viraemia. Nature *503*, 277–280.

Suloway, C., Pulokas, J., Fellmann, D., Cheng, A., Guerra, F., Quispe, J., Stagg, S., Potter, C.S., and Carragher, B. (2005). Automated molecular microscopy: the new Leginon system. J. Struct. Biol. *151*, 41–60.

Tang, G., Peng, L., Baldwin, P.R., Mann, D.S., Jiang, W., Rees, I., and Ludtke, S.J. (2007). EMAN2: an extensible image processing suite for electron microscopy. J. Struct. Biol. *157*, 38–46.

Tiller, T., Meffre, E., Yurasov, S., Tsuiji, M., Nussenzweig, M.C., and Wardemann, H. (2008). Efficient generation of monoclonal antibodies from single human B cells by single cell RT-PCR and expression vector cloning. J. Immunol. Methods *329*, 112–124.

Voss, N.R., Yoshioka, C.K., Radermacher, M., Potter, C.S., and Carragher, B. (2009). DoG Picker and TiltPicker: software tools to facilitate particle selection in single particle electron microscopy. J. Struct. Biol. *166*, 205–213.

Walker, L.M., Huber, M., Doores, K.J., Falkowska, E., Pejchal, R., Julien, J.P., Wang, S.K., Ramos, A., Chan-Hui, P.Y., Moyle, M., et al.; Protocol G Principal Investigators (2011). Broad neutralization coverage of HIV by multiple highly potent antibodies. Nature *477*, 466–470.

West, A.P., Jr., Scharf, L., Horwitz, J., Klein, F., Nussenzweig, M.C., and Bjorkman, P.J. (2013). Computational analysis of anti-HIV-1 antibody neutralization panel data to identify potential functional epitope residues. Proc. Natl. Acad. Sci. USA *110*, 10598–10603.

Wu, X., Yang, Z.Y., Li, Y., Hogerkorp, C.M., Schief, W.R., Seaman, M.S., Zhou, T., Schmidt, S.D., Wu, L., Xu, L., et al. (2010). Rational design of envelope identifies broadly neutralizing human monoclonal antibodies to HIV-1. Science *329*, 856–861.

Zhang, M.Y., Yuan, T., Li, J., Rosa Borges, A., Watkins, J.D., Guenaga, J., Yang, Z., Wang, Y., Wilson, R., Li, Y., et al. (2012). Identification and characterization of a broadly cross-reactive HIV-1 human monoclonal antibody that binds to both gp120 and gp41. PLoS One *7*, e44241.